

Trigonal field acting at the Cr^{3+} 2E states in ruby from magneto-optical measurements under high pressure

Marius Millot,¹ Jean-Marc Broto,¹ Jesus Gonzalez,² and Fernando Rodríguez^{2,*}

¹Laboratoire National des Champs Magnétiques Intenses (LNCMI), CNRS UPR 3228, Université de Toulouse, 143 Avenue de Rangueil, 31400 Toulouse, France

²MALTA Consolider Team, DCITIMAC, Facultad de Ciencias, Universidad de Cantabria, 39005 Santander, Spain

(Received 2 November 2009; revised manuscript received 5 January 2010; published 24 February 2010)

Magneto-optical measurements on ruby under high-pressure conditions provided direct determination of the trigonal crystal field acting at the t_{2g} orbitals of Cr^{3+} in Al_2O_3 (CrO_6) and its dependence with pressure. The correlation study between the measured trigonal splitting and the trigonal distortion at the Al^{3+} -substituted site indicates that the trigonal splitting increases with pressure whereas the trigonal distortion slightly reduces. The result is interpreted in terms of an enhancement of the electron-lattice coupling due to trigonal distortion upon reduction in the Al-O bond distance, i.e., the Cr-O bond distance R . The observed variations can be explained on the basis of empirical R dependence of the trigonal crystal field as $\delta V_{\text{tr}} \propto R^{-n}$ with $n=6$. It is shown that this exponent does not change when we consider the pressure variation of the local structure around Cr^{3+} obtained from *ab initio* calculations. By the way, we also demonstrate that a methanol-ethanol mixture is a good pressure transmitting medium at cryogenic temperatures.

DOI: 10.1103/PhysRevB.81.075120

PACS number(s): 78.20.Ls, 78.55.Hx

I. INTRODUCTION

Ruby (Al_2O_3 : Cr^{3+}) is a model system for optical studies in materials science and solid-state physics. The strongly efficient R_1 and R_2 photoluminescent lines arising from the lowest low-spin excited state 2E to the ground-state 4A_2 transitions make it an ideal material for crystal-field theories and applications. Besides relevant applications as first solid-state laser¹ or high-pressure gauge,^{2–8} many theoretical and experimental works were devoted to understand the unique optical properties of this material.⁸ Pioneering high-pressure spectroscopy works have shown that the Cr^{3+} crystal-field strength basically depends on the O-Al distance as R^{-5} .⁹ As a matter of fact, very recent electronic structure calculations have unveiled the role of low symmetry distortions around Cr^{3+} to explain the surprisingly high crystal-field strength responsible for its characteristic red color.^{10–12} However, trigonal-symmetry-related fine spectroscopic features revealed by high-magnetic field and high-pressure spectroscopy still deserve clarification. In fact the R_1 - R_2 splitting is a direct consequence of both the trigonal field and the spin-orbit interaction lifting the octahedral degeneracy of the 2E emitting excited state into $\bar{E}, 2\bar{A}$ spinors. However, precise information about the trigonal crystal field is hard to obtain directly from optical spectroscopy or spin resonance since it appears hidden due to low resolution or competing contribution from other interactions. We have recently shown that magneto-optical spectroscopy at low temperature under high magnetic fields and high-pressure conditions is a suitable technique to extract precise information on the trigonal component of the crystal field acting on Cr^{3+} and its variation with hydrostatic pressure.¹³ In this paper we perform a correlation study between the trigonal crystal field at Cr^{3+} sites and the associated distortion. Hence, the trigonal crystal-field pressure behavior is interpreted taking into account the variations in both the host crystal structure (Al-O bond distance

and trigonal distortion) and local structure around Cr^{3+} derived from *ab initio* calculations.^{10–12}

II. HIGH-FIELD ZEEMAN EFFECT ON RUBY R LINES

In a previous paper, we reported high-field magneto-optical measurements under high pressure on ruby single crystals up to 10 GPa and 56 T (Ref. 13) focused on the red R lines. These lines originate from radiative recombination from the two 2E states ($\bar{E}+2\bar{A}$ or $E_{1/2}+E_{3/2}$) which are two Kramers' doublets with spin 1/2 to the 4A_2 ground state with spin 3/2 ($\bar{E}+2\bar{A}$: $E_{1/2}+E_{3/2}$).¹⁴ Under high magnetic field the two emission lines are progressively divided into eight major peaks labeled A–H in Figs. 1(a) and 1(b) and four weaker ones (a, d, e, and h). This splitting can be well described by a linear Zeeman effect using Landé g factors provided by crystal-field theory^{14–16} presented in Fig. 1(c). In particular, the observed splitting between B and C lines, on the one hand, and between F and G, on the other hand, unveil the existence of two parameters Δ_1 and Δ_2 . These two parameters are the deviations of the excited state Landé factor from the value of the ground-state factor: $g_E = g_0 + 2\Delta_1$ and $g_{2A} = g_0 - 2\Delta_2$. Our measurements give direct measurement of Δ_1 and Δ_2 as indicated in Fig. 1. Under high pressure, these coefficients exhibit a significant linear increase discussed in details below. However, we will first analyze the pressure distribution on the sample in the following section in order to characterize the homogeneity of the pressure acting on the sample in the reported experiments.

III. METHANOL-ETHANOL MIXTURE AS A PRESSURE TRANSMITTING MEDIUM AT LOW TEMPERATURE

In our measurements, we used a 4:1 methanol-ethanol mixture as a pressure transmitting medium. It is well known that this medium remains hydrostatic up to 10 GPa at room

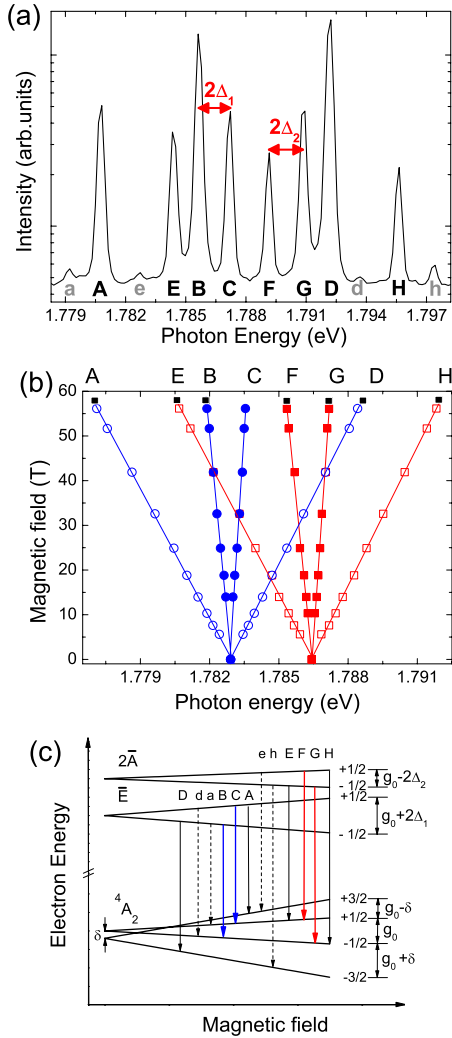


FIG. 1. (Color online) (a) Typical magneto photoluminescence spectrum of ruby at high pressure. Eight major peaks (A–H) are recorded. Logarithmic intensity scale enhances the visibility of four weaker peaks (a–h). (b) Energy Zeeman splitting fan chart enlightening the two pairs of peaks (BC) and (FG) giving direct access to Δ_1 and Δ_2 . (c) Schematic view of the Zeeman splitting of ground state (4A_2) and first excited states (2E) of ruby. Observed emission lines are described by allowed (solid arrows) and forbidden (dashed arrows) electric-dipole transitions.

temperature.^{17,18} At cryogenic temperatures, however, it is already solid even at ambient pressure and isostaticity is thereby a cumbersome issue.

Ruby is commonly used as *in situ* pressure sensor for high-pressure experiments in diamond-anvil cells using the calibration of a secondary scale.^{7,19} Its optical properties under conditions of hydrostaticity, quasi-hydrostaticity, and uniaxial stress have been intensively studied.^{3,8,20,21} Thus, we can extract a few hints about the stress distribution on the sample from zero-field high-pressure spectra. We have first examined the R_1 full width at half maximum (FWHM). At low temperature, phonon-induced broadening is weak and thus narrow lines are observed at ambient pressure ($\delta\lambda = 0.09$ nm). This width is about twice the peak width measured in ruby immersed in liquid helium.⁸ Then, pressure

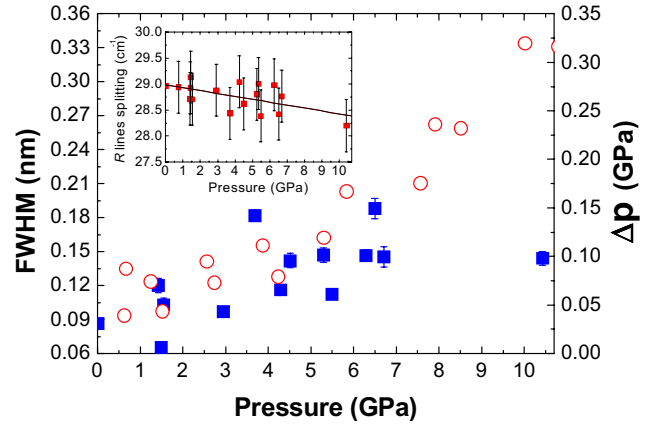


FIG. 2. (Color online) Pressure dependence of the FWHM of the R_1 line at cryogenic temperature for our single crystals (filled squares) and ruby chips dispersed in the whole pressure chamber from Ref. 22 (open circles). The right ordinate axis indicates the pressure dispersion values as calculated with equation $\Delta p = 0.5[\text{FWHM}(p) - \text{FWHM}(p_0)]/0.365$. The inset shows the pressure evolution of the R -doublet splitting at cryogenic temperature (squares). Note the slight decrease unveiled by the linear fit (solid line).

inhomogeneities throughout the sample (single crystal $150 \times 150 \times 20 \mu\text{m}^3$) can be detected by the inhomogeneous strain-induced broadening. We can estimate the pressure distribution from the FWHM of the R_1 line using $\Delta p = 0.5[\text{FWHM}(p) - \text{FWHM}(p_0)]/0.365$, where Δp refers to the standard pressure deviation and 0.365 stands for the linear pressure coefficient of the ruby R_1 line at low pressure.^{3,7,8,19–21} Figure 2 shows our experimental values for all measurements reported in Ref. 13 together with values from a recent study with ruby chips dispersed in the whole pressure chamber.²² We then obtain a pressure distribution $\Delta p < 0.15$ GPa in the explored 0–10 GPa range, which ensures fairly good quasi-hydrostatic conditions in our magneto-optical experiments.

Besides, the inset shows the evolution of the anisotropy-induced splitting between R_1 and R_2 lines. Under hydrostatic loading, this spectroscopic feature is reported to slightly decrease.^{20,23} In fact Sharma and Gupta have interpreted this evolution as a consequence of the different compressibilities along the c and a axes leading to a uniaxial strain component along the c axis under perfect hydrostatic stress.^{8,21} We find a slope of $-0.05 \pm 0.02 \text{ cm}^{-1}/\text{GPa}$ in good agreement with both estimated $-0.03 \pm 0.02 \text{ cm}^{-1}/\text{GPa}$ and measured $-0.03 \pm 0.04 \text{ cm}^{-1}/\text{GPa}$ values.²⁴ In conclusion, we can consider that the methanol-ethanol mixture is a good hydrostatic pressure transmitting medium even at cryogenic temperature. The associated inhomogeneous broadening is low enough to allow a fine spectroscopic resolution in magneto-optic experiments. Hereafter, we will then disregard any effect related to nonhydrostatic stress.

IV. TRIGONAL FIELD ENHANCEMENT UNDER HYDROSTATIC PRESSURE

As can be seen in Fig. 9 in our previous report,¹³ the pressure behavior of the Δ_1 and Δ_2 parameters extracted

from magnetophotoluminescence experiments up to 10 GPa is well described by a significant linear increase with pressure as $\Delta_1=0.23+(21\pm 3)\times 10^{-4}p$ and $\Delta_2=0.26+(25\pm 7)\times 10^{-4}p$ (Δ in g units; p in GPa). As these parameters originate from similar effects on the two ${}^2E(\bar{E}+2\bar{A})$ emitting excited states, we can summarize this behavior by $\Delta=0.25+(23\pm 5)\times 10^{-4}p=0.25\times(1+0.009p)$, or equivalently, $\frac{1}{\Delta}\frac{\partial\Delta}{\partial p}=0.009\text{ GPa}^{-1}$. From crystal-field theory, we can describe parameter Δ as the result of a third-order interaction between 2E states and higher energy states arising from 2F states involving trigonal crystal-field components and the spin-orbit coupling.^{13,15}

$$\Delta \propto \langle \bar{E}, 2\bar{A} | L_Z \times V_{\text{tr}} \times V_{\text{tr}} | {}^2F_1, {}^2F_2 \rangle + \langle \bar{E}, 2\bar{A} | S_Z \times V_{\text{tr}} \times H_{\text{SO}} | {}^2F_1, {}^2F_2 \rangle. \quad (1)$$

Hence, we can write $\kappa=\langle t_2 | V_{\text{tr}} | t_2 \rangle$ the trigonal field matrix element as¹³

$$\kappa = \left[\frac{\Delta}{12} \times (E_R - E_R') \times (E_R - E_B) \right]^{1/2}. \quad (2)$$

The R lines evolution under pressure is well known and we obtained the earliest reliable measurement of Δ through high-field magneto-optical spectroscopy under pressure.¹³ However, unlike previously reported in Eq. 6 of Ref. 13, the second and third terms were not well determined. There is only one experimental report on the R' and B lines behavior between 0 and 10 GPa (Ref. 25) and a few recent *ab initio* calculations.^{10,26} The linear dependences of these lines with pressure are:

$$\begin{aligned} E_R(\text{exp}) &= 14400 - 7.6p, & E_R(\text{calc.}) &= 14070 - 7.41p, \\ E_{R'}(\text{exp}) &= 15100 - 6.3p, & E_{R'}(\text{calc.}) &= 14820 - 7.08p, \\ E_B(\text{exp}) &= 21140 + 1.8p, & E_B(\text{calc.}) &= 21640 + 2.2p. \end{aligned} \quad (3)$$

Using these values we find from Eq. (2) that the relative variation of the trigonal energy term, $\kappa=\langle t_2 | V_{\text{tr}} | t_2 \rangle$, becomes either $\frac{1}{\kappa}\frac{\partial\kappa}{\partial p}=5.8\times 10^{-3}\text{ GPa}^{-1}$ taking the experimental pressure shifts from Ref. 25 or $\frac{1}{\kappa}\frac{\partial\kappa}{\partial p}=7.2\times 10^{-3}\text{ GPa}^{-1}$ using the calculated pressure shifts from Ref. 26. Hence, taking the mean value, our spectroscopic measurements evidence an enhancement of the trigonal crystal-field strength at the Cr³⁺ sites in ruby induced by hydrostatic pressure: $\frac{1}{\kappa}\frac{\partial\kappa}{\partial p}=(6.5\pm 0.7)\times 10^{-3}\text{ GPa}^{-1}$

V. STRUCTURAL CORRELATIONS BETWEEN TRIGONAL CRYSTAL FIELD AT Cr³⁺ AND SITE DISTORTION

In ruby, Cr³⁺ enters substitutionally at the Al³⁺ sites. Its electronic structure and fine features related to the 2E emitting excited state can be understood to a great extent on the basis of an octahedral CrO₆ unit perturbed by the trigonal distortion of the lattice and the spin-orbit interaction. Starting from an ideal O_h symmetry CrO₆ center, and using either a

conventional perturbation theory using the electronically coupled stress components of trigonal symmetry in the form of an invariant^{27,28} or an equivalent Taylor expansion of the crystal-field energy according to the Hellmann-Feynman theorem by means of normal coordinates instead of trigonal components of the strain tensor,²⁹⁻³¹ the variations in electronic energy due to trigonal crystal-field components can be expressed as:

$$\delta V = A_{11}\varepsilon_{11} = \left(\frac{\partial V}{\partial Q_t} \right)_{O_h} Q_t. \quad (4)$$

Indeed, if we consider a weak perturbation: $\varepsilon_{11}\ll 1$ or $Q_t\ll R_0$, where R_0 is the average Cr-O bond distance, the energies of the d^3 -multiplet states correspond to eigenvalues of the total Hamiltonian:

$$H(Q_t) = H_{O_h} + \left(\frac{\partial V}{\partial Q_t} \right)_{O_h} Q_t + H_{\text{S-O}}. \quad (5)$$

In the following we will refer to the trigonal components matrix elements by $\langle \delta V \rangle$ to denote the weak perturbation framework we used. The electronic wave functions acting on the electronic part of the potential energy is $\langle (\partial V / \partial Q_t)_{O_h} \rangle$. Due to highly localization of Cr³⁺ d orbitals in ruby, Q_t refers to the trigonal local coordinate around Cr³⁺ impurity that is known to be slightly different than the trigonal distortion at the Al³⁺ site in Al₂O₃.^{10-12,32} Thus, the energy or strictly speaking the matrix element $\langle \delta V \rangle$ is proportional to $\langle (\partial V / \partial Q_t)_{O_h} \rangle$ and the trigonal coordinate Q_t . The shorter the distortion is, the weaker the trigonal energy irrespective of the particular value of the electronic part.

Within crystal-field theory $(\partial V / \partial Q_t)_{O_h}$ contains terms transforming as B_2^0 , B_4^0 , and B_4^3 which depend on the Cr-O bond distance R as R^{-3} for the first term and as R^{-5} for the second and third terms.^{33,34} Although crystal-field theory is a very crude approximation to treat this problem quantitatively, we can reasonably assume that the electronic part depends on R as R^{-n} , with n being an empirical exponent describing the real dependence of $(\partial V / \partial Q_t)_{O_h}$ with R :

$$\left(\frac{\partial V}{\partial Q_t} \right)_{O_h} = KR^{-n}. \quad (6)$$

Realistic values of n are expected between 2 and 6. Interestingly, the present model is able to explain the observed variations in the trigonal field and also provides effective values of n to account for the measured shifts. On the assumption that n is positive, it turns out that $(\partial V / \partial Q_t)_{O_h}$ must increase upon reducing R , i.e., with increasing pressure.

We are interested in explaining the pressure dependence of the trigonal crystal-field matrix elements $\langle V_{\text{tr}} \rangle$, or $\langle \delta V \rangle$, which is proportional to κ [Eq. (2)] as derived from magneto-optic spectroscopy under high-pressure conditions. So that the pressure dependence of $\langle \delta V \rangle$ can be written as:

$$\begin{aligned}
\frac{\partial \langle \delta V \rangle}{\partial p} &= \frac{\partial}{\partial p} \left[\left\langle \left(\frac{\partial V}{\partial Q_t} \right)_{o_h} \right\rangle Q_t \right] \\
&= \left\langle \left(\frac{\partial^2 V}{\partial p \partial Q_t} \right)_{o_h} \right\rangle Q_t + \left\langle \left(\frac{\partial V}{\partial Q_t} \right)_{o_h} \right\rangle \frac{\partial Q_t}{\partial p} \\
&= -\frac{R_0}{3B_0} \left\langle \left(\frac{\partial^2 V}{\partial R \partial Q_t} \right)_{o_h} \right\rangle Q_t + \left\langle \left(\frac{\partial V}{\partial Q_t} \right)_{o_h} \right\rangle \frac{\partial Q_t}{\partial p}.
\end{aligned} \tag{7}$$

Using Eq. (6), we can further simplify this expression to:

$$\begin{aligned}
\frac{\partial \langle \delta V \rangle}{\partial p} &= \frac{n}{3B_0} \left\langle \left(\frac{\partial V}{\partial Q_t} \right)_{o_h} \right\rangle Q_t + \left\langle \left(\frac{\partial V}{\partial Q_t} \right)_{o_h} \right\rangle \frac{\partial Q_t}{\partial p} \\
&= \left\langle \left(\frac{\partial V}{\partial Q_t} \right)_{o_h} \right\rangle \left[\frac{n}{3B_0} Q_t + \frac{\partial Q_t}{\partial p} \right] \\
&= \langle \delta V \rangle_{\text{ruby}} \left[\frac{n}{3B_0} + \frac{1}{Q_t} \frac{\partial Q_t}{\partial p} \right].
\end{aligned} \tag{8}$$

Here $\langle \delta V \rangle_{\text{ruby}} = \langle (\partial V / \partial Q_t)_{o_h} \rangle Q_t$ represents the trigonal crystal-field energy of Cr^{3+} in ruby at ambient pressure. Therefore, there are two main contributions to $\langle \delta V \rangle$ with pressure. The first one is positive and scales with the trigonal coordinate Q_t , whereas the second term depends on how the trigonal distortion varies with pressure. If Q_t decreases with pressure then the first and the second term have different sign and partially cancel each other, while the opposite occurs if Q_t increases with pressure. Therefore, the trigonal energy increases with pressure provided that Q_t increases. Nevertheless, the opposite does not imply necessary energy decrease with pressure unless $n/3B_0 < (1/Q_t)(\partial Q_t / \partial p)$.

In order to verify which option applies to ruby we must compare the relative variation of Q_t with pressure and $n/3B_0$. Unfortunately there are no data relative to the variation in local structure around Cr^{3+} in ruby from pressure experiments due to current limitations to perform suitable extended x-ray-absorption fine structure (EXAFS) measurements under pressure in diluted Al_2O_3 : Cr^{3+} (0.5 mol %). However, this limitation can be mitigated using structural data available for the Al^{3+} site as a function of pressure and calculations of $R_{\text{Al-O}}$ and $R_{\text{Cr-O}}$ as a function of pressure. Although we know that Cr^{3+} and Al^{3+} local coordination geometries are different, $R_{\text{Al-O}} = 1.86$ and 1.97 Å ($R_{\text{Al-O}}^{\text{avg}} = 1.915$ Å) from x-ray diffraction³⁵ and $R_{\text{Cr-O}} = 1.92$ and 2.02 Å ($R_{\text{Cr-O}}^{\text{avg}} = 1.965$ Å) from EXAFS at ambient conditions,^{36,37} we can initially assume that their pressure variations are similar. In fact, Fig. 3 shows the calculated pressure dependence of volume for AlO_6 and CrO_6 in ruby taken from Ref. 10. The different compressibilities of both octahedra are evident at very high pressures ($p > 20$ GPa). However, their relative variations are similar below about 20 GPa. This noteworthy result implies that the R^{-5} law found for the crystal-field splitting $10Dq$ as a function of $R_{\text{Al-O}}^{\text{avg}}$ (Ref. 9) should be identical if we analyze $10Dq$ as a function of $R_{\text{Cr-O}}^{\text{avg}}$ instead of $R_{\text{Al-O}}^{\text{avg}}$. This argument also applies to the trigonal distortion although its variation with pressure for CrO_6 should be

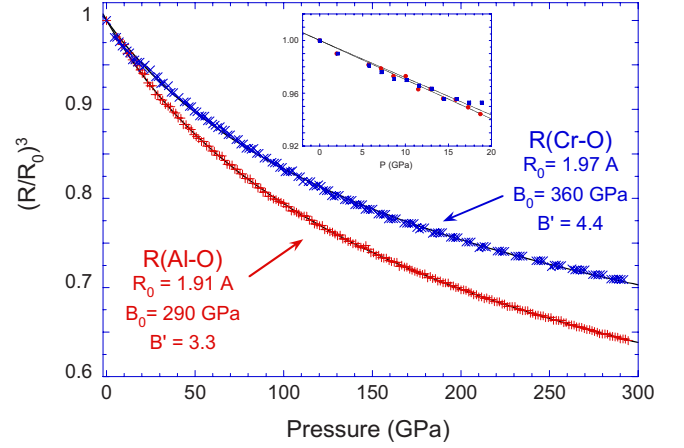


FIG. 3. (Color online) Pressure dependence of $(R/R_0)^3$ for both Al-O and Cr-O distances in Al_2O_3 : Cr^{3+} in the 0–300 GPa range obtained from *ab initio* calculations in Ref. 10. The parameters correspond to the local bulk modulus and its derivative B' derived by fitting the average $(R/R_0)^3$ values which have been calculated for Al-O and Cr-O (Ref. 10) to a Murnaghan's equation of state (MEOS). Although MEOS is crude to derive actual values of the bulk modulus and its pressure derivative, the fit parameters reflect a bigger compressibility of the AlO_6 octahedron with respect to CrO_6 at high pressure. However, their relative variation is similar for Al-O and Cr-O within 10% of accuracy in the 0–20 GPa range. Inset: magnification of the low pressure region showing a linear dependence with slopes of 3.0×10^{-3} and 2.8×10^{-3} GPa^{-1} for Al-O and Cr-O, respectively.

slightly higher than AlO_6 .¹⁰ In particular, we can show that the variation in Q_t is nearly homothetic with pressure for both Al^{3+} and Cr^{3+} .

The trigonal distortion of the AlO_6 octahedron in Al_2O_3 can be described from structural data by the expression:

$$r/a = 1/3 - v(\text{O}) = 0.027, \tag{9}$$

where r is the displacement of the oxygen along the trigonal axis according to a description given elsewhere,³⁸ $v(\text{O})$ is the reduced coordinate of the oxygen in the corundum, and a is the hexagonal lattice parameter. Note that r/a is zero in a perfect AlO_6 octahedron ($v = 1/3$). However, this is not the case for Al_2O_3 with $v = 0.306$.⁸

The corresponding trigonal strain components are:

$$\begin{aligned}
\varepsilon_{11} = \varepsilon_{22} &= -3r/4a = -0.0203, \\
\varepsilon_{33} &= \frac{c}{2\sqrt{2}a} - 1 = -0.0347.
\end{aligned} \tag{10}$$

Here the axial component depends on the variation in the c/a ratio but ε_{11} and ε_{22} depend on the variation in the internal coordinate $v(\text{O})$. These data are known from XRD experiments under pressure and therefore the pressure dependence of the trigonal distortion variation can be precisely evaluated.^{35,39–42}

Up to 4.6 GPa, it is known that $v(\text{O})$ varies from 0.3061 at ambient pressure to 0.3065 at 4.1 GPa with an almost linear dependence in the whole pressure range. It implies that

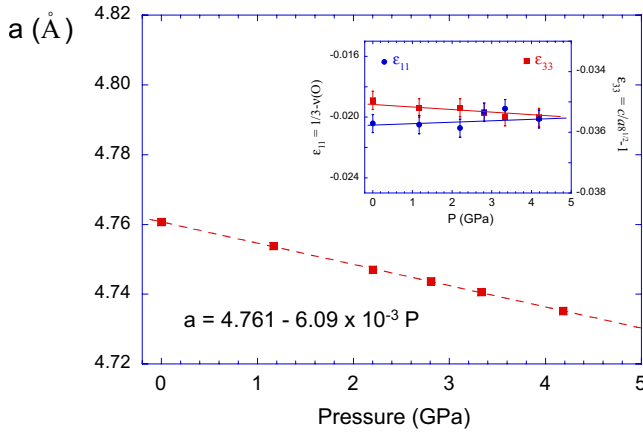


FIG. 4. (Color online) Variation in the hexagonal lattice parameter a with pressure obtained from x-ray diffraction (Ref. 39). The inset shows the corresponding variation in the trigonal strain parameters ϵ_{11} and ϵ_{33} derived from structural data from Refs. 39–42.

$\frac{1}{u(O)} \frac{\partial u(O)}{\partial p} = 3 \times 10^{-4} \text{ GPa}^{-1} \approx 0$ within the experimental accuracy, i.e., that relative trigonal distortion ϵ_{11} slightly decreases with pressure while ϵ_{33} increases thus yielding to an effective relative trigonal strain distortion smaller than 10^{-3} GPa^{-1} (Fig. 4). Therefore we conclude that the trigonal strain is homothetic with pressure and therefore the associated trigonal coordinate decreases with pressure owing to the scaling: $Q_t \sim \epsilon_{11} a$.

Hence, the relative variation of Q_t is equal to the relative variation of the lattice parameter a , and we obtain from Fig. 4:

$$\frac{1}{Q_t} \frac{\partial Q_t}{\partial p} = \frac{1}{a \epsilon_{11}} \frac{\partial a \epsilon_{11}}{\partial p} = \frac{1}{a} \frac{\partial a}{\partial p} \approx -1.3 \times 10^{-3}. \quad (11)$$

The trigonal homotheticity is in agreement with XRD measurements by Holzapfel *et al.*³⁵ who established that the coordinate $u(O)=0.352$ does not vary between ambient pressure and 9 GPa. If we take into account the dispersion of XRD data on this figure, we conclude that within the experimental uncertainty ϵ_{11} does not change significantly with pressure.

Now by comparing the second term of Eqs. (8) and (11) with the first term $n/(3B_0)$, we obtain $n/3B_0=2.6 \times 10^{-3} \text{ GPa}^{-1}$ for $n=2$ and $n/3B_0=7.8 \times 10^{-3} \text{ GPa}^{-1}$ for $n=6$ using the bulk modulus value $B_0=253.7 \text{ GPa}$ given in Ref. 43. Therefore, this first term represents a major contribution to the trigonal energy variation even in the less favorable case of $n=2$ at least two times larger than the second

term contribution if the trigonal parameter is given by Eq. (11). The same conclusion is reached if we consider the local Q_t around Cr^{3+} although calculations predict that the trigonal field around Cr^{3+} varies with pressure slightly higher than for Al^{3+} leading to local variations in trigonal distortion that are pretty small: $(1/Q_t)(\partial Q_t/\partial p) \approx 0$.¹⁰

The experimental variation in κ , which is given by $\frac{1}{\kappa} \frac{\partial \kappa}{\partial p} = 6.5 \times 10^{-3} \text{ GPa}^{-1}$, indicates that the trigonal crystal field increases with pressure even if Q_t decreases due to volume reduction [Eq. (11)]. The increase in κ is consistent with the proposed model by the increase in the trigonal coupling parameter $(\partial V/\partial Q_t)$ with pressure on the assumption of R dependence as R^{-n} [Eq. (6)]. Hence, we can determine $n/3B_0$ empirically through Eqs. (8) and (11) and thus the exponent as $n=(6.5 \times 10^{-3} + 1.3 \times 10^{-3})3B_0=6.0 \pm 1.0$. This value accidentally agrees with the exponent derived from crystal-field theory but is obtained from magneto-optical spectroscopy, thus, providing experimental evidence of a R^{-6} law for the trigonal crystal field at Cr^{3+} in ruby.

VI. CONCLUSIONS

The magneto-optical spectra of the ruby R lines can be interpreted in terms of variation in the trigonal crystal field with pressure taking into account two main contributions: one implicit which is associated with changes in the coupling parameter with pressure at constant distortion, Q_t , and one explicit contribution which is related to variations in Q_t with pressure and constitutes a minor contribution in ruby. The measured variation in the trigonal crystal-field energy κ can be described by means of a pressure dependence of the coupling parameter $(\partial V/\partial Q_t)_{O_h}$ as R^{-6} in agreement with predictions based on crystal-field theory. It must be also noted that the empirical exponent ($n=6$) is similar to that describing the dependence of the octahedral crystal-field splitting $10Dq$ with pressure as $10Dq \propto R^{-5}$ using the Al-O bond distance $R_{\text{Al-O}}$ instead of $R_{\text{Cr-O}}$ but this can be *a posteriori* justified by recent *ab initio* estimates on the pressure-induced variation revealing that the relative variation of $R_{\text{Al-O}}$ and $R_{\text{Cr-O}}$ is similar in the 0–10 GPa range.

ACKNOWLEDGMENTS

Financial support from the Spanish Ministerio de Ciencia e Innovación (Project No. MAT2008-06873-C02-01), MALTA INGENIO-CONSOLIDER 2010 (Grant No. CDS2007-0045), and EuroMagnet II FP7 program are acknowledged.

*Corresponding author. rodriguf@unican.es

¹T. H. Maiman, *Nature* (London) **187**, 493 (1960).

²R. A. Forman, G. J. Piermarini, J. D. Barnett, and S. Block, *Science* **176**, 284 (1972).

³J. H. Eggert, K. A. Goettel, and I. F. Silvera, *Phys. Rev. B* **40**, 5724 (1989).

⁴J. H. Eggert, F. Moshary, W. J. Evans, K. A. Goettel, and I. F. Silvera, *Phys. Rev. B* **44**, 7202 (1991).

⁵W. B. Holzapfel, *J. Appl. Phys.* **93**, 1813 (2003).

⁶J. Lin, O. Degtyareva, C. T. Prewitt, P. Dera, N. Sata, E. Gregoryanz, H. Mao, and R. J. Hemley, *Nature Mater.* **3**, 389 (2004).

⁷A. D. Chijioko, W. J. Nellis, A. Soldatov, and I. Silvera, *J. Appl.*

- Phys. **98**, 114905 (2005).
- ⁸K. Syassen, High Press. Res. **28**, 75 (2008).
- ⁹H. G. Drickamer and C. W. Frank, *Electronic Transitions and the High Pressure Chemistry and Physics of Solids* (Chapman and Hall, London, 1973).
- ¹⁰W. Duan, G. Paiva, R. M. Wentzcovitch, and A. Fazzio, Phys. Rev. Lett. **81**, 3267 (1998).
- ¹¹J. M. García-Lastra, M. T. Barriuso, J. A. Aramburu, and M. Moreno, Phys. Rev. B **72**, 113104 (2005).
- ¹²S. Watanabe, T. Sasaki, R. Taniguchi, T. Ishii, and K. Ogasawara, Phys. Rev. B **79**, 075109 (2009).
- ¹³M. Millot, J. M. Broto, and J. Gonzalez, Phys. Rev. B **78**, 155125 (2008).
- ¹⁴S. Sugano, Y. Tanabe, and H. Kamimura, *Multiplets of Transition-Metal Ions* (Academic, New York, 1970).
- ¹⁵S. Sugano and Y. Tanabe, J. Phys. Soc. Jpn. **13**, 880 (1958).
- ¹⁶S. Sugano and I. Tsujikawa, J. Phys. Soc. Jpn. **13**, 899 (1958).
- ¹⁷G. J. Piermarini, S. Blockland, and J. D. Barnett, J. Appl. Phys. **44**, 5377 (1973).
- ¹⁸S. Klotz, J.-C. Chervin, P. Munsch, and G. Le Marchand, J. Phys. D **42**, 075413 (2009).
- ¹⁹A. F. Goncharov, J. M. Zaug, J. C. Crowhurst, and E. Gregoryanz, J. Appl. Phys. **97**, 094917 (2005).
- ²⁰M. Chai and J. M. Brown, Geophys. Res. Lett. **23**, 3539 (1996).
- ²¹S. M. Sharma and Y. M. Gupta, Phys. Rev. B **43**, 879 (1991).
- ²²N. Tateiwa and Y. Haga, AIRAPT 22 Conference [J. Phys.: Conf. Ser. (to be published)].
- ²³J. M. Besson and J. P. Pinceaux, Rev. Sci. Instrum. **50**, 541 (1979).
- ²⁴R. G. Munro, G. J. Piermarini, S. Block, and W. B. Holzapfel, J. Appl. Phys. **57**, 165 (1985).
- ²⁵R. A. Forman, B. A. Weinstein, and G. Piermarini, *Spectroscopie des Éléments de Transition et des Éléments Lourds Dans les Solides* (Colloques Internationaux Centre National de la Recherche Scientifique, Paris, 1977), Vol. 255, p. 51.
- ²⁶D. P. Ma, H. M. Zhang, Y. Y. Liu, J. R. Chen, and N. Ma, J. Phys. Chem. Solids **60**, 463 (1999).
- ²⁷A. A. Kaplyanskii, Opt. Spectrosc. **16**, 329 (1964).
- ²⁸A. A. Kaplyanskii and A. K. Przhdevskii, Sov. Phys. Solid State **9**, 190 (1967).
- ²⁹R. Valiente and F. Rodriguez, Phys. Rev. B **60**, 9423 (1999).
- ³⁰F. Rodriguez, G. Davies, and E. C. Lightowers, Phys. Rev. B **62**, 6180 (2000).
- ³¹F. Aguado, F. Rodriguez, and P. Nuñez, Phys. Rev. B **67**, 205101 (2003).
- ³²S. J. Duclos, Y. K. Vohra, and A. L. Ruoff, Phys. Rev. B **41**, 5372 (1990).
- ³³K. A. Schroeder, J. Chem. Phys. **37**, 2553 (1962).
- ³⁴R. M. Macfarlane, J. Chem. Phys. **39**, 3118 (1963).
- ³⁵H. d'Amour, D. Schiferl, W. Denner, H. Schulz, and W. B. Holzapfel, J. Appl. Phys. **49**, 4411 (1978).
- ³⁶E. Gaudry, D. Cabaret, C. Brouder, I. Letard, A. Rogalev, F. Wilhlem, N. Jaouen, and P. Sainctavit, Phys. Rev. B **76**, 094110 (2007).
- ³⁷E. Gaudry, A. Kiratisin, P. Sainctavit, C. Brouder, F. Mauri, A. Ramos, A. Rogalev, and J. Goulon, Phys. Rev. B **67**, 094108 (2003).
- ³⁸J. F. Clare and S. D. Devine, J. Phys. C **13**, 865 (1980).
- ³⁹H. V. Hart and H. G. Drickamer, J. Chem. Phys. **43**, 2265 (1965).
- ⁴⁰L. W. Finger and R. M. Hazen, J. Appl. Phys. **49**, 5823 (1978).
- ⁴¹Y. Sato and S. Akimoto, J. Appl. Phys. **50**, 5285 (1979).
- ⁴²J. Kim-Zajonz, S. Werner, and H. Schulz, Z. Kristallogr. **214**, 331 (1999).
- ⁴³T. Goto, O. L. Anderson, T. Ohno, and S. Yamamoto, J. Geophys. Res. **94**, 7588 (1989).